This article has been accepted for publication in IEEE Access. This is the author's version which has not been fully edited and content may change prior to final publication. Citation information: DOI 10.1109/ACCESS.2024.3404016

IEEE Access
Multidisciplinary : Rapid Review : Open Access Journal

Date of publication xxxx 00, 0000, date of current version xxxx 00, 0000.

Digital Object Identifier 10.1109/ACCESS.2022.Doi Number

MaskLRF: Self-supervised Pretraining via Masked Autoencoding of Local Reference Frames for Rotation-invariant 3D Point Set Analysis

Takahiko Furuya[1]

[1]Integrated Graduate School of Medicine, Engineering, and Agricultural Sciences, University of Yamanashi, 4-3-11 Takeda, Kofu-shi, Yamanashi-ken, 400-8511, Japan

Corresponding author: Takahiko Furuya (e-mail: takahikof@yamanashi.ac.jp).

This work was supported by the Japan Society for the Promotion of Science (JSPS) KAKENHI (Grant No. 21K17763).

ABSTRACT Following the successes in the fields of vision and language, self-supervised pretraining via masked autoencoding of 3D point set data, or Masked Point Modeling (MPM), has achieved state-of-the-art accuracy in various downstream tasks. However, current MPM methods lack a property essential for 3D point set analysis, namely, invariance against rotation of 3D objects/scenes. Existing MPM methods are thus not necessarily suitable for real-world applications where 3D point sets may have inconsistent orientations. This paper develops, for the first time, a rotation-invariant self-supervised pretraining framework for practical 3D point set analysis. The proposed algorithm, called MaskLRF, learns rotation-invariant and highly generalizable latent features via masked autoencoding of 3D points within Local Reference Frames (LRFs), which are not affected by rotation of 3D point sets. MaskLRF enhances the quality of latent features by integrating feature refinement using relative pose encoding and feature reconstruction using low-level but rich 3D geometry. The efficacy of MaskLRF is validated via extensive experiments on diverse downstream tasks including classification, segmentation, registration, and domain adaptation. The experiments demonstrate that MaskLRF achieves new state-of-the-art accuracies in analyzing 3D point sets having inconsistent orientations. Code will be available at: https://github.com/takahikof/MaskLRF.

INDEX TERMS 3D point cloud, deep learning, masked autoencoding, representation learning, self-supervised pretraining.

I. INTRODUCTION

Deep learning is an essential technique for accurate 3D point set analysis. Notably, in recent years, self-supervised pretraining of Deep Neural Networks (DNNs) for 3D point sets has become one of the hottest research topics in 3D vision [1], [2]. Self-supervised pretraining leverages a large amount of unlabeled 3D point sets instead of labeled ones, which are often difficult to collect due to high labeling costs. The typical framework of self-supervised pretraining first trains an encoder DNN, or backbone, via a pretext task using unlabeled 3D point sets as training data. The pretrained backbone is then finetuned for specific downstream tasks by using (usually small amount of) labeled 3D point sets. Accuracies for downstream tasks highly depend on the pretext task used for pretraining.

Following the successes of masked language modeling [3] and masked image modeling [4], [5], there has been a growing interest in masked autoencoding of 3D point sets, also referred to as Masked Point Modeling (MPM) [6]. MPM is a pretext task where a DNN reconstructs a set of erased, or masked, local regions from an incomplete input 3D point set consisting of unmasked 3D points. The recently proposed MPM methods ([6], [7], [8], [9], [10], [11]) employ Transformer [12] as a backbone DNN for its capability to refine local shape features considering their interrelationships. These MPM methods thus can acquire expressive latent 3D shape features that capture both local shape geometry and global shape context, leading to state-of-the-art accuracy in 3D point set analysis.

However, the existing MPM methods have a drawback;

they are not invariant to SO(3) rotations of 3D point sets. The previous studies on MPM use 3D point sets whose orientations are consistently aligned by humans, at all the stages of pretraining, finetuning, and evaluation. I argue that such a strongly constrained setup is not always practical since orientations of 3D point sets are generally inconsistent in real-world application scenarios. For example, the orientations of scanned real-world 3D objects can vary depending on the poses of both an object and a range scanner. Or, the correspondence between the upright direction of a synthetic 3D shape and one of the three axes of a coordinate system depends on 3D modeling software. The existing MPM methods thus end up in limited use cases.

This paper aims at developing a practical and versatile self-supervised pretraining framework for 3D point set analysis. To this end, I propose a novel rotation-invariant (RI) MPM algorithm called *MaskLRF* (Fig. 1). The core idea of MaskLRF is simple; It normalizes the orientation of each local region of a 3D point set by using Local Reference Frame (LRF) [4], [13], and performs masked autoencoding on a set of rotation-normalized local regions.

However, designing a Transformer-based RI MPM framework is non-trivial due to the following two issues. First, I cannot use (absolute) positional encoding [6], which is not only essential for feature refinement but also serves as a "prompt" for 3D shape reconstruction. The positional encoding used by the existing MPM methods is a rotation-covariant quantity that changes with rotation of 3D points, and thus is not suitable for RI MPM. Second, a proper reconstruction target is not clear since there is no prior work on RI MPM. Some recent studies on non-RI MPM [11], [14], [15] found that reconstructing weakly encoded low-level features instead of raw 3D points leads to better latent features. In light of these findings, the reconstruction target for RI MPM should also be chosen carefully.

To address the first issue, I propose *relative pose encoding*, which describes both relative position and relative orientation among local regions of a 3D point set. The relative pose encoding is an RI quantity. Therefore, it realizes MPM of 3D point sets having inconsistent orientations. For the second issue, I assume that the finding by the non-RI MPM algorithms [11], [14], [15] is also valid for RI MPM. That is, reconstructing features that describe low-level but rich 3D geometry of rotation-normalized local

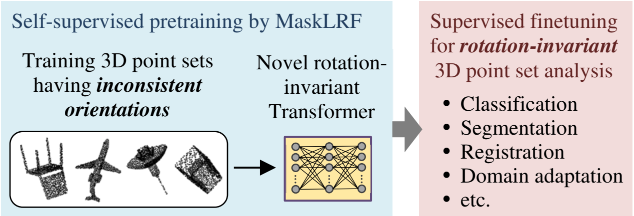

FIGURE 1. This paper proposes a self-supervised pretraining framework tailored to rotation-invariant (RI) analysis of 3D point sets. The parameters of the pretrained RI Transformer are used as initialization of finetuning for diverse downstream tasks.

regions will enhance the quality of latent features. Based on this assumption, MaskLRF employs a handcrafted shape feature having 3D grid structure as the reconstruction target.

The effectiveness of MaskLRF is verified on various downstream tasks including real-world object classification, few-shot object classification, part segmentation, scene registration, and domain adaptation. The experiments show that MaskLRF achieves new state-of-the-art accuracies in analyzing 3D point sets having inconsistent orientations.

Contributions of this paper are summarized as follows.

- Developing a first-of-its-kind self-supervised pretraining framework specialized for *rotation-invariant* (RI) analysis of 3D point sets.
- Proposing a novel Masked Point Modeling (MPM) framework called MaskLRF. It accepts rotationally inconsistent 3D point sets at all stages of pretraining, finetuning, and evaluation. MaskLRF thus extends potential use cases of the current Transformers for 3D point set, which do not have rotation invariance.
- Comprehensively evaluating the effectiveness of MaskLRF. It achieves accuracy higher than existing MPM methods and existing RI DNNs in analyzing 3D point sets having inconsistent orientations.

II. RELATED WORK

A. SELF-SUPERVISED PRETRAINING FOR 3D POINT SET ANALYSIS

Self-supervised pretraining enables DNNs to learn general-purpose feature representations which can be transferred to various downstream tasks. A number of self-supervised pretraining algorithms for 3D point set analysis have been proposed [1], [2]. Among them, promising methods can be categorized into two approaches, i.e., contrastive learning-based ([16], [17], [18], [19]) and MPM-based ([6], [7], [8], [9], [10], [11], [14], [15], [20], [21], [22]) approaches.

PointContrast by Xie et al. [16] is the pioneering work of the contrastive learning-based approach. [16] employs a pretext task that compares latent 3D shape features extracted from randomly augmented two 3D point set scenes. Zhang et al. [17] propose to use multi-view depth maps as training data for self-supervised pretraining. Depth maps are converted to two different shape representations (i.e., point sets and voxels) and are processed by a DNN for contrasting their latent shape features. Rao et al. [18] propose a contrastive learning using synthetic 3D point set scenes instead of using scanned 3D scenes. Long et al. [19] contrast the latent features extracted by a DNN with the prototype latent features acquired by clustering, both at the point-level and object-level.

The pretext task by Han et al. [22], called half-to-half reconstruction, can be viewed as an early generation MPM. In [22], a 3D object is split into two partial 3D point sets having nearly equal size and a DNN is trained by reconstructing one of the partial 3D point sets from the other partial 3D point set given as an input. Wang et al. [21] create incomplete 3D point sets by masking all the occluded 3D points when a synthetic 3D point set is viewed from a certain perspective. The DNN of [21] is trained so that it complements the occluded points of an incomplete 3D point set. These early generation MPM algorithms [21], [22], however, use an inadequately expressive backbone DNN such as PointNet [24] or its variant [23], which makes pretraining less effective.

To improve the MPM framework, Transformer model [12] was introduced as a new backbone DNN. The typical learning procedure for the Transformer-based MPM is as follows. Firstly, an input training 3D point set is split into multiple local regions and a certain percentage of the local regions are masked. The unmasked, or visible, regions are then described as feature vectors called tokens. Transformer takes as its input the set of visible tokens and refines the tokens by using the self-attention mechanism [12] that is capable of considering interrelationships among the tokens. Transformer is trained so that it reconstructs 3D point sets within masked local regions.

Point-BERT by Yu et al. [6] and Point-MAE by Pang et al. [8] are the first Transformer-based MPM algorithms that employ the abovementioned learning procedure. Point-BERT and Point-MAE have outperformed most of the existing contrastive learning-based methods and the early generation MPM methods in various downstream tasks. Therefore, the Transformer-based MPM can currently be positioned as the state-of-the-art approach for self-supervised pretraining for 3D point set analysis. More recent studies have attempted to improve the Transformer-based MPM by introducing, for example, hierarchical Transformer architecture [9], discriminative pretext task [7], and autoregressive generative pretext task [11]. As mentioned in Section I, however, all the existing Transformer-based MPM do not have invariance against SO(3) rotations of 3D point sets. They are thus not suitable for downstream tasks that require rotation invariance. In contrast, this paper is unique since it realizes RI Transformer-based MPM to extend potential use cases.

Apart from the abovementioned single-modal approaches that use only 3D point set data, some studies [25], [26], [27], [28], [29] have attempted to leverage knowledge of different modalities, e.g., 2D image and/or text. [28] and [29] employ a vision-language model (e.g., CLIP [30]) to improve both masking strategy and pretext task of the Transformer-based MPM. Note that the use of knowledge from different data domain is beyond the scope of this paper. My study falls into a single-modal Transformer-based MPM approach; I use only 3D point set data to obtain rotation-invariant and highly generalizable latent 3D shape features.

B. ROTATION-INVARIANT 3D POINT SET ANALYSIS

Rotation invariance is essential for practical 3D point set analysis. Various RI DNNs for 3D point sets have been proposed. They can be classified into the following three approaches; extracting inherently RI feature ([31], [32], [33], [34], [35], [36], [37]), designing rotation-equivariant DNN architecture ([38], [39]), and normalizing rotation of 3D point sets ([40], [41], [42], [43], [44], [45], [46], [47]).

Extracting inherently RI feature. The group of prior studies [31], [32], [33], [34], [35], [36], [37] have used 3D geometric features that are not affected by the rotation of input 3D point sets. These methods sample local regions of a 3D point set at the initial layer of a DNN. The local regions are encoded using RI low-level features, such as distances between 3D points and angles among surface normals. These RI local features are then propagated through subsequent layers to generate an object-level RI feature. While being inherently RI, encoding to low-level features such as distances and angles results in a significant loss of 3D shape information.

Designing rotation-equivariant DNN architecture. Shen et al. [38] and Deng et al. [39] have extend DNN neurons from 1D to 3D so that they can preserve SO(3) rotation of the input 3D point set. Such rotation-equivariant shape features are converted to RI features by computing inner product of two identical rotation-equivariant shape features [39] or taking the norms of 3D neurons [38]. However, as noted by [35], the rotation-equivariant DNNs need to impose strong constraints, such as linearity, on their layers to achieve rotation equivariance, sacrificing flexibility in feature extraction.

Normalizing rotation. The studies in this category achieve rotation invariance by normalizing the orientation of a 3D point set at global scale [37], [42] or local scale [40], [43], [47]. Compared to global scale, rotation normalization at local scale is easier since 3D shape in a local region tends to be simple. Furuya et al. [40] compute a local coordinate system called Local Reference Frame (LRF) to rotation-normalize each local region. The LRF of [40] is computed by applying Principal Component Analysis (PCA) to the 3D points within a local region. Specifically, three mutually orthogonal axes for rotation normalization are computed by eigendecomposition of the covariance matrix of the 3D points in a local region. Luo et al. [43] and Zhang et al. [47] propose a DNN block that predicts an intrinsic LRF of a local region for its rotation-normalization. The use of LRF achieves rotational invariance without loss of 3D shape information in a local region. I thus considered LRF to be a suitable means for RI MPM. As the first attempt of RI MPM, this paper employs a well-studied, PCA-based LRF.

All the existing RI DNNs described above assume to be supervisedly trained from scratch without pretraining. Self-supervised pretraining of RI DNNs has not yet been studied. Spezialetti et al. [48] and Kim et al. [49] proposed self-supervised pretext tasks that predict canonical orientation of 3D point sets. However, these methods are not rigorously rotation invariant since they employ non-RI DNNs. Recently,

This article has been accepted for publication in IEEE Access. This is the author's version which has not been fully edited and content may change prior to final publication. Citation information: DOI 10.1109/ACCESS.2024.3404016

Spezialetti et al. [50] and Furuya et al. [51] introduced self-supervised learning of fully rotation-invariant 3D point set features. However, their methods are designed not for pretraining, but for a specific task such as registration or retrieval. In contrast, my method is versatile; it acquires highly generalizable RI features useful for various downstream tasks.

III. PROPOSED ALGORITHM

A. OVERVIEW OF PROPOSED ALGORITHM

Section III elaborates MaskLRF, which bridges the state-of-the-art self-supervised pretraining (i.e., Transformer-based MPM) to rotation-invariant 3D point set analysis. Fig. 2 illustrates the overview of MaskLRF. Hereafter, a local region cropped from a 3D point set is called a patch. A training 3D point set is first divided into visible patches and masked patches, each of which is associated with an LRF. The visible patches are rotation-normalized and then embedded as token features by the DNN layers. For token refinement, I design *Relative pose-aware Rotation-invariant Point Transformer (R2PT)*. R2PT has three differences compared to the Transformers used in the previous MPM methods. (i) R2PT incorporates relative pose encoding into the attention computation to consider mutual pose differences between rotation-normalized patches. (ii) R2PT effectively and efficiently captures both local geometry and global context of a 3D point set by alternately applying local attention and global yet sparse attention. (iii) The entire DNN is effectively pretrained via the pretext task that involves reconstruction of handcrafted 3D grid-structured features extracted from masked patches. After pretraining by MaskLRF, the encoder part of R2PT is finetuned for downstream tasks.

B. PATCHIFICATION AND MASKING

MaskLRF employs a patchification procedure similar to the existing MPM methods [6], [8]. A training 3D point set $\mathbf{X}$ consists of n oriented 3D points where each 3D point is associated with its normal vector. The center 3D points of N_p patches are obtained by applying Farthest Point Sampling (FPS) [23] to $\mathbf{X}$. Each patch is formed by collecting k 3D points closest to its center point $\mathbf{c}$. A set of 3D points within a patch is represented as a matrix $\mathbf{S} \in \mathbb{R}^{k \times 3}$. To obtain invariance against translation, 3D points within $\mathbf{S}$ are represented by normalized coordinates with respect to its center point $\mathbf{c}$. Throughout this paper, n, N_p, and k for pretraining are fixed at 1,024, 64, and 32, respectively. The patches may thus spatially overlap each other.

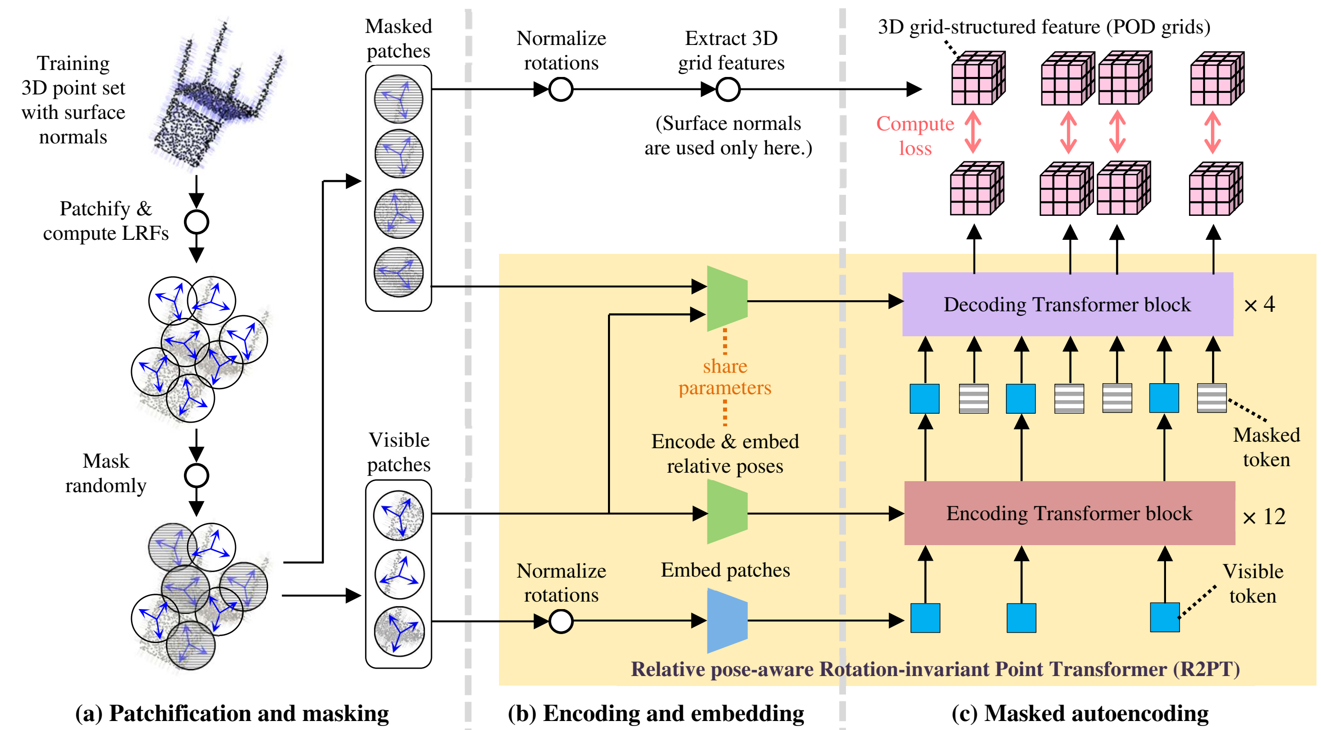

FIGURE 2. The overview of MaskLRF. (a) A training 3D point set is divided into multiple patches, each of which is associated with its Local Reference Frame (LRF). A certain percentage (e.g., 60%) of the patches is randomly masked. (b) Every visible/masked patch is rotation-normalized by using its LRF. Each visible patch is then embedded by the DNN layers while each masked patch is described by a shape feature having 3D grid structure. Relative poses among the patches are encoded by using their positions and LRFs. (c) The entire DNN is trained via the masked autoencoding task where the DNN is forced to reconstruct the 3D grid-structured features of the masked patches. The Transformer blocks effectively refine the tokens by simultaneously considering their feature similarities and relative poses.

For each patch, MaskLRF computes an LRF, which consists of three mutually orthogonal axes $\mathbf{e}_1$, $\mathbf{e}_2$, and $\mathbf{e}_3$. Computation of LRF has been well studied in the literature [52], [53], [54]. In this paper, the first axis $\mathbf{e}_1$ is obtained by applying PCA to the covariance matrix of $\mathbf{S}$. $\mathbf{e}_1$ corresponds to the eigenvector associated with the smallest eigenvalue. The sign of $\mathbf{e}_1$ is disambiguated by using the method in [55]. $\mathbf{e}_1$ estimates the normal of an object surface. Note that the surface normal associated with $\mathbf{X}$ is not used as $\mathbf{e}_1$, so that MaskLRF can process 3D point sets without normals in finetuning and evaluation. The second axis is obtained as in [35]. That is, $\mathbf{e}_2$ is computed by projecting the vector from the center point $\mathbf{c}$ to the barycenter of the patch onto the plane perpendicular to $\mathbf{e}_1$. The third axis $\mathbf{e}_3$ is computed as the cross product of $\mathbf{e}_1$ and $\mathbf{e}_2$. The LRF is represented as a 3×3 matrix $\mathbf{F}$, whose column corresponds to one of $\mathbf{e}_1$, $\mathbf{e}_2$, and $\mathbf{e}_3$. As a result, each patch P is represented as a triplet ($\mathbf{S}$, $\mathbf{c}$, $\mathbf{F}$).

For masking, MaskLRF employs the same strategy as in [6], [8]. Specifically, M % of N_p patches are randomly chosen as masked patches, and the remaining patches are treated as visible patches. In the experiments, the masking ratio M during pretraining is set to 60. The influence of M on the accuracy of a downstream task is evaluated in the experiments. At the finetuning stage, masking is not performed. That is, all the N_p patches are treated as visible ones.

C. RELATIVE POSE-AWARE ROTAION-INVARIANT POINT TRANSFORMER (R2PT)

Relative pose encoding and its embedding. Relative pose encoding attempts to compensate for the loss of pose information caused by normalizing rotations of the patches. In the encoder block of R2PT, a relative pose encoding is computed for every pair of visible patches cropped from the 3D point set $\mathbf{X}$. The decoder block, on the other hand, computes relative pose encodings among all the visible/masked patches of $\mathbf{X}$. A relative pose encoding comprises two quantities, i.e., relative position and relative orientation. Let a pair of two patches be $P_i = (\mathbf{S}_i, \mathbf{c}_i, \mathbf{F}_i)$ and $P_j = (\mathbf{S}_j, \mathbf{c}_j, \mathbf{F}_j)$. The relative position RP_{ij} and relative orientation RO_{ij} of P_i with respect to P_j are calculated by Eq. 1 and 2, respectively.

$$\mathrm{RP}_{ij} = \left(\mathbf{c}_i - \mathbf{c}_j\right)\mathbf{F}_j\,, \quad \mathrm{RP}_{ij} \in \mathbb{R}^3 \tag{1}$$

$$\mathrm{RO}_{ij} = \mathbf{F}_i^T\,\mathbf{F}_j\,, \quad \mathrm{RO}_{ij} \in \mathbb{R}^{3\times 3} \tag{2}$$

RP_{ij} denotes the position of $\mathbf{c}_i$ in the LRF $\mathbf{F}_j$ whose origin is $\mathbf{c}_j$, while RO_{ij} corresponds to the rotation matrix that aligns $\mathbf{F}_i$ with $\mathbf{F}_j$ [55]. RP_{ij} and RO_{ij} are constant regardless of any rotation of $\mathbf{X}$. RP_{ij} and RO_{ij} are then flattened and concatenated to obtain a 12D relative pose encoding vector. The 12D vector is embedded in higher-dimensional space by using the two-layer MLP. The parameters of this MLP are shared across all the encoding/decoding Transformer blocks

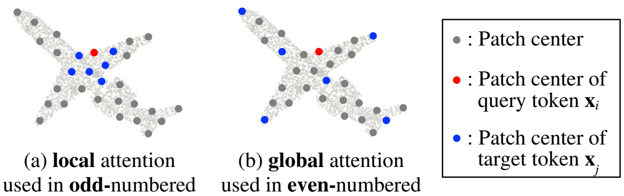

(a) **local** attention used in **odd**-numbered Transformer blocks

(b) **global** attention used in **even**-numbered Transformer blocks

FIGURE 3. R2PT effectively and efficiently captures both local shape geometry and global shape context of a 3D point set by alternately applying the local and global self-attention.

in R2PT. The relative pose embedding, denoted as $\mathbf{R}_{ij} \in \mathbb{R}^d$ ($d = 384$), is used for the self-attention computation described below.

Encoder part. Each visible patch P_i is rotation-normalized by computing $\mathbf{S}_i\,\mathbf{F}_i$. The patch is then converted to a token feature $\mathbf{x}_i \in \mathbb{R}^d$ by the PointNet [24]-like DNN, as in [6], [7], and [8]. The encoder part is a series of 12 Transformer blocks. Each block takes as input a set of tokens ($\mathbf{x}_1$, ..., $\mathbf{x}_{N_v}$) and outputs a set of refined tokens ($\mathbf{y}_1$, ..., $\mathbf{y}_{N_v}$) where $\mathbf{y}_i \in \mathbb{R}^d$. N_v is the number of visible tokens, which is equal to $(1-M/100)\times N_p$ for pretraining and N_p for finetuning.

A typical self-attention requires a spatial and temporal complexity of $O(N_v^2)$. In addition to attention computation, MaskLRF requires the same complexity for relative pose embedding. The encoder works efficiently during pretraining since N_v is small. In contrast, however, finetuning suffers from high complexity. To reduce the cost, I propose to subsample attention target tokens. This paper employs two types of self-attention, i.e., local attention to capture local shape geometry (Fig. 3a) and global attention to capture long-range shape context (Fig. 3b). For each query token $\mathbf{x}_i$, local attention collects, in the 3D space, t nearest neighbors as attention targets for $\mathbf{x}_i$. Global attention obtains t attention targets for $\mathbf{x}_i$ by applying FPS to the patch center points. Inspired by [57] for 2D image analysis, local attention is used in the odd-numbered Transformer blocks and global attention is used in the even-numbered Transformer blocks. Such an alternate block arrangement is expected to progressively refine the tokens considering both local geometry and global context at a low computation cost. For pretraining, t is set to N_v /4. t for finetuning is fixed at 16 regardless of N_p, which varies depending on a downstream task.

After subsampling the attention targets, each query token $\mathbf{x}_i$ is refined by the relative pose-aware self-attention:

$$\mathbf{y}_i = \sum_{j \in \varphi(\mathbf{x}_i)} \alpha_{ij}\mathbf{v}_{ij} \tag{3}$$

In Eq. 3, $\varphi(\mathbf{x}_i)$ denotes a set of indices for the attention targets of $\mathbf{x}_i$. α_{ij} and $\mathbf{v}_{ij}$ are the attention score and value vector between tokens $\mathbf{x}_i$ and $\mathbf{x}_j$, respectively. Note that not only α_{ij} but also $\mathbf{v}_{ij}$ reflects the relation between the tokens. α_{ij} and $\mathbf{v}_{ij}$ are computed by the following equations.

$$\mathbf{v}_{ij} = \mathbf{x}_j \mathbf{W}^{\mathrm{V}} + \mathbf{R}_{ij} \quad (4)$$

$$\alpha_{ij} = \exp(e_{ij}) \Big/ \sum_{l \in \varphi(\mathbf{x}_i)} \exp(e_{il}) \quad (5)$$

$$e_{ij} = \frac{(\mathbf{x}_i \mathbf{W}^{\mathrm{Q}})(\mathbf{x}_j \mathbf{W}^{\mathrm{K}})^T + (\mathbf{x}_i \mathbf{W}^{\mathrm{Q}})\, \mathbf{R}_{ij}^T}{\sqrt{d}} \quad (6)$$

In the equations, the terms colored in green hold relative pose information. Omitting the green terms boils down to the original self-attention [12]. $\mathbf{W}^{\mathrm{Q}}$, $\mathbf{W}^{\mathrm{K}}$, $\mathbf{W}^{\mathrm{V}} \in \mathbb{R}^{d \times d}$ are linear projections with learnable parameters. I use six heads for multi-head self-attention. The set of refined tokens is further processed by an MLP with skip connection as in [12], and is fed into the subsequent Transformer block.

Decoder part. The decoder part comprises four Transformer blocks. Each block receives N_v visible tokens and N_m masked tokens ($N_m = N_p - N_v$). The initial masked token, which is a d-dimensional learnable vector, is duplicated N_m times and input to the first decoding block. Each decoding block refines a total of N_p tokens by using the relative-pose aware self-attention as in the encoder part. The refined masked tokens from the last decoding block are further processed by a single-layer prediction head to reconstruct the set of feature vectors denoted as ($\mathbf{z}_1$, ..., $\mathbf{z}_{Nm}$).

D. OBJECTIVE OF PRETRAINING

Reconstruction target. Most MPM methods employ a pretext task that needs to reconstruct raw 3D point sets within masked patches. More recent studies found that reconstructing weakly encoded features, such as surface variations [20] or binary occupancy grids [14], [15], leads to effective pretraining. This paper proposes to reconstruct more expressive 3D geometric features. The reconstruction target of MaskLRF is represented as a 3D grid-structured feature, which describes low-level but rich 3D geometry. Specifically, the bounding box of each rotation-normalized masked patch is spatially partitioned by 6×6×6 regular grids. Each grid cell is described by a 10D feature called POD [58], which consist of the frequency (1D), the mean coordinates (3D), and the covariance of normal vectors (6D). The 3D grid feature is then flattened to obtain a feature vector $\hat{\mathbf{z}}_i$ having 6×6×6×10 = 2160D. Note that the surface normals of a training sample are only used to extract its POD features.

Intuition behind POD grid reconstruction. MaskLRF does not reconstruct raw 3D point sets since shapes of rotation-normalized patches are less diverse compared to those of non-normalized patches used by the non-RI MPM methods. In the non-RI MPM methods, even simple patches (e.g., rods or planes) can have various orientations, making diverse local shapes available for pretraining. In contrast, patches of MaskLRF are less diverse since the 3D points in a patch are rotation-normalized by using the fixed rule described in Section III.B. In this case, the DNN can easily reduce the loss for point set reconstruction by generating simple (e.g., elliptical or planar) shapes having a specific orientation. As a result, the pretraining may converge to a suboptimal solution. This paper thus proposes the POD grid reconstruction to effectively train the DNN using patches with limited shape diversity. The POD grid reconstruction imposes the following challenging pretext task on the DNN: "Are cells within a 3D grid occupied by points? If so, predict the 3D geometric features within that cell". In other words, the proposed reconstruction task requires jointly solving two predictive tasks, i.e., occupancy prediction and geometric feature prediction, which facilitate learning of better latent shape features.

Loss and optimization. The loss for each training 3D point set is calculated by Eq. 7.

$$L = \sum_{i=1}^{N_m} \| \mathbf{z}_i - \hat{\mathbf{z}}_i \|_2^2 \quad (7)$$

AdamW [59] is used for optimization. The learning rate is initialized at 10^{-3} and is decreased to 10^{-6} by using a cosine scheduling. Pretraining is iterated for 300 epochs with the batch size of 64. During pretraining (and also in finetuning), each training sample is augmented by random anisotropic scaling with scaling ratios ranging from 0.8 to 1.2.

E. FINETUNING

After pretraining, the decoder part of R2PT is replaced with a task-specific prediction head whose parameters are initialized randomly. The parameters of the entire DNN are then finetuned. In the process of prediction, each task-specific prediction head computes different types of 3D shape features, i.e., global features and pointwise features, depending on the downstream task.

Global features are mainly used for classification tasks. Each encoding block of R2PT is expected to capture shape features at different semantic levels due to the alternate local/global block arrangement. All refined tokens are thus used for a global feature. Specifically, at each of the 12 encoding blocks, output tokens are aggregated by average pooling. The resultant 12 aggregated tokens are then concatenated to create a global feature per 3D point set.

Pointwise features are used for tasks that require per-point prediction, such as segmentation and registration. The token features output from the last encoding Transformer block are upsampled to pointwise features. This paper adopts Pose-aware Feature Propagation devised in [47] for upsampling. This module leverages not only distances among neighboring 3D points but also angles among LRFs.

The finetuning also uses AdamW. The learning rate increases linearly from 0 to η during the first 10 epochs. After the 10-th epoch, it decreases toward 0 by using a cosine scheduling. The hyperparameters used for finetuning are presented in Section IV-A.

IV. EXPERIMENTS AND RESULTS

A. EXPERIMENTAL SETUP

The effectiveness of MaskLRF is verified on five downstream tasks of 3D point set analysis, i.e., real-world object classification, few-shot object classification, part segmentation, scene registration, and domain adaptation.

Competitors. The experiments on the classification and segmentation tasks use existing self-supervised pretraining methods as competitors. They are six MPM-based methods [6], [7], [8], [9], [10], [11]. In addition, previously proposed DNNs having rotation invariance [35], [36][1], [37], [39], [40], [42], [43], [45], [47], [60] are included in the set of competitors. These RI DNNs are not pretrained, but are trained from scratch for each downstream task. Furthermore, I add pretrained RI DNNs to the competitors for a fair evaluation. Specifically, the two state-of-the-art RI DNNs [36], [47] are pretrained by using the state-of-the-art self-supervised representation learning algorithm for 3D point set called SDMM [51]. SDMM is built upon the self-distillation framework [61] originally proposed for 2D images. On the other hand, the experiments on the scene registration and domain adaptation tasks compare MaskLRF with existing methods specifically designed for each task.

Dataset for pretraining. For a fair comparison, all the pretraining methods, including MaskLRF, use the ShapeNetCore55 dataset [62] for self-supervised pretraining. ShapeNetCore55 contains over 50,000 3D shapes categorized into 55 semantic classes. Note that the category labels are not used for self-supervised pretraining. Each 3D point set consists of n = 1,024 points.

Rotation settings. To evaluate rotation invariance of the methods, the experiments use three rotation settings, i.e., A/A, A/R, and R/R. "A" stands for "consistently aligned", while "R" means "randomly rotated". The A/A setting uses 3D point sets whose orientations are consistently aligned by humans at all the stages of pretraining, finetuning, and evaluation. A/A is the easiest setting, but would not fit to real-world application scenarios. In the A/R setting, pretraining and finetuning use consistently aligned 3D point sets while evaluation uses randomly rotated 3D point sets. R/R uses randomly rotated 3D point sets throughout pretraining, finetuning, and evaluation. RI methods should produce similar accuracy values in the three rotation settings. Note that identical accuracy values are not expected even for RI methods due to randomness in DNN training.

Hyperparameters for finetuning. Table I shows the hyperparameter values used for each downstream task. For the number of epochs for classification and segmentation, I follow the evaluation protocol of the existing studies [6], [8]. The number of patches N_p is set larger for the segmentation and registration tasks since they require pointwise dense prediction.

[1] Since the official code of RIConv++ [36] did not exhibit rotation invariance, I modified it to be rotation-invariant.

TABLE I. Hyperparameters of MaskLRF used for finetuning. (b: batch size, e: number of epochs, η: initial learning rate, N_p: number of patches per 3D shape, k: number of 3D points contained in a patch, t: number of attention targets per token).

Downstream tasks	b	e	η	N_p	k	t
Real-world object classification	32	300	5×10^{-5}	128	32	16
Few-shot object classification	32	150	5×10^{-4}	128	32	16
Part segmentation	24	300	5×10^{-5}	256	32	16
Scene registration	1	20	5×10^{-5}	1,024	32	16
Domain adaptation	32	30	5×10^{-6}	128	32	16

B. COMPARISON AGAINST EXISTING ALGORITHMS

Real-world object classification. I use two benchmark datasets consisting of scanned 3D objects, i.e., ScanObjectNN (SONN) [63] and OmniObject3D (OO3D) [64]. SONN consists of 2,890 indoor objects classified into 15 categories. I use the official train/test split with 2,309 training shapes and 581 testing shapes. This paper reports accuracies for the three subsets of SONN, i.e., OBJ_BG, OBJ_ONLY, and PB_T50_RS. The OO3D dataset consists of 5,382 3D point sets classified into 216 diverse categories. Since no official train/test split is provided, I select roughly 80% of the dataset for training and the rest for testing, resulting in 4,219 training shapes and 1,163 testing shapes.

Table II demonstrates the effectiveness of MaskLRF. For all the four datasets, the existing MPM algorithms suffer from significant accuracy drop especially under the A/R setting. This is because the previous MPM framework does not have rotation invariance. The previously proposed RI DNNs exhibit rotation invariance, but their accuracies are inferior to MaskLRF. Pretraining of the previous RI DNNs performs better than training from scratch, but its improvement is marginal. In contrast, MaskLRF yields better accuracies, indicating that it acquires expressive RI features during pretraining with the help of relative pose encoding and 3D grid feature reconstruction. Interestingly, MaskLRF outperforms the existing MPM methods even under the A/A setting. This is probably because the orientations of 3D point sets in the datasets are not perfectly aligned. MaskLRF having rotation invariance is advantageous in that it can avoid the problem of orientation misalignment.

Few-shot object classification. I follow the evaluation protocol in [65]. [65] adopts "K-way N-shot" classification scenarios. It randomly selects K classes from the ModelNet40 dataset [66], and then (N+20) samples are randomly chosen for each class. A DNN is trained on K×N samples and tested on the remaining K×20 samples. I conduct 10 independent experiments and report their average classification accuracy as in [65].

Table III shows accuracies for "5-way 10-shot", "5-way 20-shot", "10-way 10-shot", and "10-way 20-shot" scenarios.

TABLE II. Accuracies [%] for the real-world 3D object classification task. (Pre.: self-supervised pretraining, RI: rotation invariance)

Methods	Pre.	RI	SONN OBJ_BG dataset			SONN OBJ_ONLY dataset			SONN PB_T50_RS dataset			OO3D dataset		
			A/A	A/R	R/R	A/A	A/R	R/R	A/A	A/R	R/R	A/A	A/R	R/R
PointBERT [6]	✓		87.4	32.4	86.1	88.1	29.2	86.0	83.1	23.9	81.7	70.9	9.3	70.4
MaskPoint [7]	✓		89.3	29.0	87.6	88.1	29.1	85.9	84.3	25.4	82.9	72.8	9.1	70.5
Point-MAE [8]	✓		90.2	26.5	88.3	88.2	29.9	87.7	85.2	24.7	84.4	71.4	9.1	70.5
Point-M2AE [9]	✓		91.2	32.8	86.3	88.8	32.5	85.7	86.4	28.8	80.7	72.1	13.4	69.4
MaskSurf [10]	✓		91.2	29.0	89.2	89.2	31.2	87.6	85.8	26.1	84.6	72.3	9.3	70.7
PointGPT [11]	✓		91.6	31.5	85.4	90.0	31.6	85.2	**86.9**	25.5	80.6	71.7	9.7	57.9
DLAN [40]		✓	82.6	82.9	82.8	82.2	82.5	82.0	74.9	75.0	74.9	66.3	66.5	66.3
PoseSelector [42]		✓	80.6	80.5	80.9	82.3	81.4	81.9	76.1	75.8	75.8	63.7	63.8	64.0
VN-DGCNN [39]		✓	69.8	70.1	69.7	71.1	70.6	72.1	64.3	64.7	65.3	51.9	52.1	51.6
LGR-Net [37]		✓	85.1	85.2	85.3	85.2	85.7	85.6	77.1	76.6	76.6	69.0	68.7	69.0
EOMP [43]		✓	75.6	75.3	75.8	75.6	76.4	75.8	67.4	69.2	68.0	53.6	54.3	54.3
PaRI-Conv [35]		✓	87.4	87.3	86.6	84.3	84.8	84.7	82.3	82.3	82.4	68.1	68.2	67.9
RIConv++ [36]		✓	89.7	90.0	89.7	88.8	88.3	88.0	85.4	85.2	85.3	71.2	70.9	71.1
PaRot [47]		✓	88.2	88.5	88.0	85.3	85.3	85.8	82.3	82.5	82.6	70.9	70.8	70.9
RIConv++ & SDMM	✓	✓	90.2	90.4	90.2	88.8	89.0	88.6	85.3	85.2	84.8	71.5	71.7	71.3
PaRot & SDMM	✓	✓	90.7	90.7	90.6	88.4	88.8	88.7	83.6	83.8	83.6	73.1	73.3	72.5
MaskLRF (proposed)	✓	✓	**93.1**	**93.1**	**93.3**	**90.2**	**90.1**	**89.8**	86.7	**86.7**	**86.8**	**76.5**	**76.6**	**76.8**

TABLE III. Accuracies [%] for the few-shot 3D object classification task using the ModelNet40 few-shot dataset. (Pre.: self-supervised pretraining, RI: rotation invariance)

Methods	Pre.	RI	5-way 10-shot			5-way 20-shot			10-way 10-shot			10-way 20-shot		
			A/A	A/R	R/R	A/A	A/R	R/R	A/A	A/R	R/R	A/A	A/R	R/R
PointBERT [6]	✓		94.6	53.0	91.5	96.3	49.7	95.3	91.0	32.0	85.9	92.7	33.7	90.9
MaskPoint [7]	✓		95.0	45.0	90.4	97.2	48.3	95.6	91.4	29.4	84.8	93.4	29.5	89.5
Point-MAE [8]	✓		96.3	52.6	87.7	97.8	50.9	93.7	92.6	33.6	80.2	95.0	33.3	88.4
Point-M2AE [9]	✓		**96.8**	58.0	89.1	98.3	58.1	94.5	92.3	39.2	83.6	95.0	38.6	89.5
MaskSurf [10]	✓		96.5	50.9	90.9	98.0	49.5	95.0	**93.0**	33.0	83.3	**95.3**	31.6	90.2
PointGPT [11]	✓		**96.8**	48.2	84.3	**98.6**	49.8	93.8	92.6	30.2	79.6	95.2	28.2	87.2
DLAN [40]		✓	90.7	91.1	90.5	95.2	94.8	94.6	84.8	85.2	85.0	90.2	90.1	90.5
PoseSelector [42]		✓	83.4	79.2	82.7	90.1	85.3	89.7	78.0	71.7	75.0	86.9	82.0	85.9
VN-DGCNN [39]		✓	62.2	66.2	62.0	79.0	78.0	78.4	51.7	51.4	46.6	65.3	65.0	63.0
LGR-Net [37]		✓	88.9	89.1	89.4	92.9	93.2	93.2	81.3	81.5	81.7	89.9	89.9	89.6
EOMP [43]		✓	36.9	37.5	37.0	78.3	77.2	75.9	54.6	49.4	44.7	71.7	69.3	72.3
PaRI-Conv [35]		✓	89.9	90.7	90.5	94.6	95.0	94.5	84.6	84.6	84.0	90.9	90.7	91.0
RIConv++ [36]		✓	87.3	87.9	87.5	93.3	93.4	92.9	80.0	79.8	79.9	88.6	88.9	88.7
PaRot [47]		✓	46.9	52.2	49.0	70.5	72.2	73.6	50.9	48.3	46.2	58.9	64.1	63.9
RIConv++ & SDMM	✓	✓	91.2	91.0	91.1	94.6	94.8	94.6	85.4	85.3	85.0	91.4	91.3	91.6
PaRot & SDMM	✓	✓	93.3	93.2	93.3	95.5	96.2	96.2	88.2	88.6	88.3	92.1	93.0	92.7
MaskLRF (proposed)	✓	✓	93.5	**93.6**	**93.8**	96.4	**96.5**	**96.4**	89.2	**89.5**	**89.5**	93.6	**93.7**	**93.7**

In Table III, MaskLRF yields superior classification accuracy over the existing RI DNNs. This result suggests that MaskLRF is better at mitigating overfitting during finetuning when labeled training samples are scarce. As in the real-world object classification experiment, the existing MPM methods show lower classification accuracy in the A/R and R/R settings compared to the A/A setting. This indicates that existing MPM methods have difficulty in acquiring rotation invariance in the few-shot classification scenario.

Part segmentation. I use the ShapeNetPart dataset [67], which contains 16,881 3D objects categorized into 16 semantic classes. I follow the evaluation protocol in [24]. That is, MaskLRF computes both global feature and pointwise feature described in Section III-E. Each pointwise feature is concatenated with the global feature and object class label, and then processed by an MLP to produce a pointwise prediction. Category-level mean Intersection-over-Union (C-mIoU) [24] is used as an accuracy index.

As shown in Table IV, the proposed MaskLRF clearly outperforms the existing methods under the A/R and R/R settings. This result implies that MaskLRF is capable of learning highly semantic pointwise features even when the orientations of the 3D shapes are inconsistent. Table V shows

TABLE IV. Accuracies (C-mIoU [%]) for the part segmentation task.

Methods	Pre.	RI	ShapeNetPart dataset		
			A/A	A/R	R/R
Point-MAE [8]	✓		84.2	38.7	79.4
Point-M2AE [9]	✓		**84.9**	41.1	80.2
MaskSurf [10]	✓		84.4	38.4	81.7
PointGPT [11]	✓		84.1	38.8	79.4
LGR-Net [37]		✓	80.0	80.0	80.1
RMGnet [60]		✓	–	81.5	81.4
AECNN [45]		✓	80.2	80.2	80.2
RIConv++ [36]		✓	–	80.3	80.3
PaRot [47]		✓	–	79.2	79.5
RIConv++ & SDMM	✓	✓	80.2	80.3	80.3
PaRot & SDMM	✓	✓	80.3	80.3	80.4
MaskLRF (proposed)	✓	✓	83.2	**83.4**	**83.5**

TABLE V. Category-wise mean IoU [%] for the part segmentation task under the R/R setting.

Methods	aero	bag	cap	car	chair	earph.	guitar	knife	lamp	laptop	motor	mug	pistol	rocket	skate	table
Point-MAE [8]	82.0	79.8	83.8	74.0	89.2	70.3	90.2	**86.3**	82.1	81.6	66.6	92.2	79.7	59.2	72.7	80.6
Point-M2AE [9]	82.9	79.9	82.4	75.0	89.6	72.8	90.9	85.0	83.4	83.7	71.0	93.7	80.8	57.6	74.1	81.1
MaskSurf [10]	83.0	79.5	84.6	76.8	89.9	74.7	91.1	85.6	83.7	**89.1**	72.0	92.5	82.6	**66.1**	74.5	80.6
PointGPT [11]	80.3	78.7	83.0	69.9	89.1	79.9	90.1	85.0	83.6	84.6	62.7	92.1	80.1	56.4	74.6	80.9
LGR-Net [37]	81.7	78.1	82.5	75.1	87.6	74.5	89.4	86.1	83.0	86.4	65.3	92.6	75.2	64.1	**79.8**	80.5
RMGnet [60]	82.4	81.0	85.7	76.9	89.7	79.7	91.5	84.1	81.9	84.7	72.6	93.8	81.9	61.4	77.5	79.5
PaRot [47]	82.9	82.1	83.2	75.7	89.4	76.1	91.5	86.1	81.4	80.3	59.3	94.3	79.7	57.0	73.3	79.2
RIConv++ & SDMM	83.1	81.0	87.7	77.5	90.3	65.5	90.8	84.8	82.9	82.3	69.0	94.3	79.1	54.7	73.7	**81.3**
PaRot & SDMM	83.9	77.8	86.0	75.9	89.3	74.0	91.3	85.5	82.4	81.2	68.7	93.9	78.6	57.7	75.1	80.1
MaskLRF (proposed)	**85.2**	**84.5**	**88.9**	**80.0**	**90.5**	**80.6**	**91.6**	84.8	**84.6**	86.9	**76.7**	**95.4**	**82.8**	64.6	77.7	**81.3**

mean IoU for each object category. MaskLRF outperforms the existing methods in 12 out of 16 object categories.

Scene registration. Rotation invariance is essential for scene registration [68], [69]. As in [68], I use the rotated variant of the 3DMatch [70] and 3DLoMatch [71] datasets. These datasets include 62 indoor scenes, among which 46 are used for training, 8 for validation, and 8 for evaluation. A pair of scenes in 3DMatch and 3DLoMatch has >30% and 10-30% spatial overlap, respectively. As evaluation indices, I use Inlier Ratio (IR) [72] which measures an accuracy of point correspondence, and Registration Recall (RR) [70] that quantifies a success rate of registration. To adapt MaskLRF to the scene registration task, I replace the encoder and decoder of RoITr [69] with the pretrained encoder part of R2PT and the randomly initialized upsampling module mentioned in Section III-E, respectively. The entire DNN is then finetuned as in [69].

Table VI compares registration accuracies for rotated 3D point set scenes. As shown in Table VI, MaskLRF outperforms the existing DNN architectures specifically designed for scene registration. In particular, significant improvement in IR is observed. This result supports the claim in the part segmentation task; MaskLRF succeeds in obtaining highly semantic pointwise features.

TABLE VI. Accuracies (IR [%] and RR [%]) for registration of rotated 3D point set scenes.

Methods	3DMatch dataset		3DLoMatch dataset	
	IR	RR	IR	RR
YOHO [73]	53.5	92.4	19.2	64.5
RIGA [68]	70.7	92.6	34.3	67.0
GeoTrans [74]	73.3	91.8	42.7	72.0
RoITr [69]	82.6	94.4	55.1	76.6
MaskLRF (proposed)	**86.4**	**94.6**	**60.3**	**77.6**

Domain adaptation. This subsection evaluates the capability of domain adaptation by MaskLRF. I use the adaptation scenario [75] from the synthetic 3D shape domain (source) to the real-world 3D shape domain (target). The source dataset consists of synthetic 3D point sets created from polygonal 3D shapes in the ModelNet10 (MN10) [66] or ShapeNet10 (SN10) [75] datasets. The target dataset consists of realistic 3D point sets in the ScanNet10 dataset [75] obtained by scanning real-world objects. After pretraining by MaskLRF, the proposed R2PT is trained to classify the object categories in the source dataset. Quality of domain adaptation is measured by classification accuracy for the target dataset. In addition to the synthetic/realistic domain gap, I observed that 3D shapes in the source and target domains had different upright orientations. Existing domain adaptation methods [75], [76], [77], [78], [79], [80] [81] preprocess the 3D shapes so that their upright axes are consistently aligned. However, such prior knowledge cannot be used for unknown datasets. Hence, I argue that rotation invariance is also essential for domain adaptation of 3D point sets.

Table VII compares classification accuracy on the target domain dataset. It is worth noting that MaskLRF which requires no upright orientation alignment produces the accuracy competitive to the existing methods that involve upright alignment. The result suggests that pretraining by MaskLRF is beneficial to domain adaptation, indicating high transferability of the learned RI features.

TABLE VII. Accuracies [%] for the domain adaptation task.

Methods	MN10 → ScanNet10	SN10 → ScanNet10
PointDAN [75]	44.8	45.7
DefRec [76]	42.6	46.1
GAST [77]	54.9	53.6
MLSP [78]	55.4	55.6
ImplicitPCDA [79]	55.3	55.4
GLRV [80]	53.6	49.1
PC-Adapter [81]	**58.2**	53.7
MaskLRF (proposed)	55.5	**55.7**

C. IN-DEPTH EVALUATION OF MASK-LRF

This section verifies the effectiveness of each component of MaskLRF. The evaluation in this section uses classification accuracy [%] on the OBJ_BG subset of SONN and the OO3D dataset under the R/R rotation setting.

Reconstruction target. Table VIII compares reconstruction targets for pretraining. Evidently, the proposed POD grids lead to higher accuracy compared to the reconstruction targets devised in the previous studies. As mentioned in III-D, the proposed POD grid reconstruction imposes two challenging prediction tasks, i.e., occupancy prediction and geometric feature prediction. Jointly solving these two pretext tasks has a positive impact on the self-supervised pretraining of the proposed DNN. This is supported by the fact that the reconstruction of POD girds

This article has been accepted for publication in IEEE Access. This is the author's version which has not been fully edited and
content may change prior to final publication. Citation information: DOI 10.1109/ACCESS.2024.3404016

outperforms the reconstruction of occupancy grids [14], [15], which involves the occupancy prediction only. Table VIII also includes the results of the existing MPM methods whose reconstruction target is replaced with POD grids. The proposed POD grid reconstruction brings a slight but consistent improvement to pretraining by the existing MPM methods.

TABLE VIII. Comparison of reconstruction targets for MPM.

Methods	Reconstruction targets	OBJ_BG	OO3D
MaskLRF (proposed)	3D points [6], [8], [9], [11]	88.5	72.4
	3D points with normal [10]	90.5	73.9
	FPFH feature [11]	90.4	73.4
	Surface variations [20]	72.6	49.9
	Occupancy grids [14], [15]	91.9	75.8
	POD grids (proposed)	**93.3**	**76.8**
Point-MAE (A/A setting)	3D points	90.2	71.4
	POD grids (proposed)	90.5	73.3
Point-M2AE (A/A setting)	3D points	91.2	72.1
	POD grids (proposed)	92.0	73.1

Fig. 4 exemplifies results of masked autoencoding by MaskLRF after pretraining. For visualization, raw 3D point sets are used as the reconstruction targets. Fig. 4 shows that MaskLRF successfully reconstructs the masked 3D points regardless of rotations of the input 3D shape, implying that MaskLRF acquires expressive RI latent features.

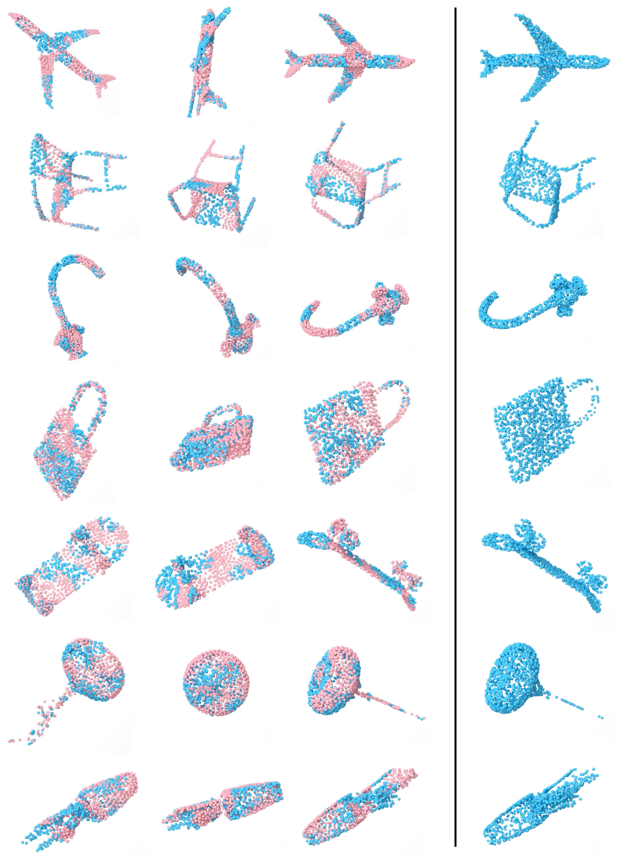

FIGURE 4. Examples of masked autoencoding by MaskLRF. In each row, the left three 3D point sets are reconstruction results for different orientations of the same 3D object. Visible (unmasked) points and predicted points are colored in blue and pink, respectively. The rightmost 3D point set is the groundtruth for its adjacent reconstruction result.

Relative pose encoding. I conduct an ablation study on the proposed relative pose encoding. In Table IX, "None" is the case that does not use relative pose information. That is, the green terms in Eq. 4 and 6 are omitted during pretraining and finetuning. "RP only" and "RO only" use either one of relative pose (Eq. 1) and relative orientation (Eq. 2). Table IX demonstrates that using both RP and RO contributes to effective pretraining. Without relative pose encoding, positional and orientational relationship among tokens cannot be used for feature refinement, resulting in significant accuracy drop.

Table IX. Effectiveness of relative pose encoding.

Relative pose encoding	OBJ_BG	OO3D
None	81.3	65.2
RP only	93.1	76.0
RO only	87.6	73.0
Both RP and RO (proposed)	**93.3**	**76.8**

Local/global self-attention. Table X demonstrates the efficacy of combining local and global self-attention. Local attention alone fails to capture global context of 3D shape, while global attention alone has difficulty in describing local geometry. I also experiment a variant where the first half of the encoder/decoder part uses local attention only and the latter half uses global attention only. Table 8 shows that alternating local/global attentions enables effective feature refinement, resulting in high transferability to the downstream task.

Table X. Effectiveness of combining local/global attentions.

Self-attention	OBJ_BG	OO3D
Local attention only	90.1	74.0
Global attention only	90.3	74.2
First half: local & latter half: global	91.5	76.3
Alternating local/global attention (proposed)	**93.3**	**76.8**

Amount of data for pretraining. Table XI shows the influence of data amount for pretraining on the accuracy of the downstream task. In Table XI, "100%" uses all the ~50,000 samples of ShapeNetCore55 for pretraining. "0%" does not perform pretraining and the DNN is trained from scratch for the downstream task. Interestingly, even a pretraining with only 1% (~500) samples has a positive impact on the accuracy in the downstream task. This result indicates that the DNN architecture and pretext task of MaskLRF are appropriately designed for self-supervised

Table XI. Influence of amount of data for MaskLRF pretraining.

Amount of data for pretraining	OBJ_BG	OO3D
0 % (no pretraining)	75.7	56.4
1 %	83.1	70.5
5 %	83.6	70.8
10 %	89.4	72.9
50 %	92.0	74.9
100 % (all samples in ShapeNetCore55)	**93.3**	**76.8**

This article has been accepted for publication in IEEE Access. This is the author's version which has not been fully edited and
content may change prior to final publication. Citation information: DOI 10.1109/ACCESS.2024.3404016

pretraining. Table XI also shows that classification accuracy improves as the amount of data increases. The result implies that more (>50,000) data leads to more accurate latent 3D shape features. I leave pretraining using larger datasets and/or larger DNN models for my future work.

Masking ratio. Table XII shows the impact of the masking ratio *M* during pretraining on the downstream task. The peak of the classification accuracy appears at around the masking ratio of 50-60%. These masking ratios are similar to those employed by the existing non-RI MPM methods (e.g., [8]). Decreasing *M* approaches a simple autoencoding framework without masking. Using a too small *M* (e.g., 10%) only forces the DNN to learn an identity mapping, which does not lead to learning of meaningful latent 3D shape features. On the other hand, using too large *M* (e.g., 90%) makes the pretext task too difficult. Too few visible patches hamper the inference of an entire 3D shape to be reconstructed by the DNN, resulting in the low accuracy as shown in Table XII.

Table XII. Influence of the masking ratio *M* for pretraining.

Masking ratio *M*	OBJ_BG	OO3D
10 %	92.1	74.8
20 %	92.3	75.3
30 %	92.8	76.1
40 %	93.0	76.1
50 %	**93.4**	76.6
60 %	93.3	**76.8**
70 %	92.8	75.4
80 %	91.5	74.1
90 %	88.8	73.4

V. CONCLUSION AND FUTURE WORK

A. CONCLUSION

This paper tackled, for the first time, a rotation-invariant (RI) framework of self-supervised pretraining for 3D point set analysis. The proposed Masked Point Modeling (MPM) algorithm, called MaskLRF, learns RI latent shape features via masked autoencoding of local patches whose rotations are normalized by their Local Reference Frames. MaskLRF refines rotation-normalized patches by using self-attention layers with relative pose encoding, which can consider mutual pose differences among the patches. The pretext task that requires to reconstruct 3D grid-structured descriptors having rich 3D geometry facilitates to learn expressive latent features. The efficacy of MaskLRF was verified via extensive experiments on various downstream tasks. In addition, the in-depth evaluation validated the design of the proposed algorithm. These experiments revealed that MaskLRF is capable of learning rotation-invariant and highly generalizable latent 3D shape features in a self-supervised learning framework. More specifically:

- Although MaskLRF uses synthetic 3D point sets derived from 3D CAD models for pretraining, the learned latent features are effective in analyzing real-world (noisy) 3D point sets with inconsistent orientations, as shown in the experiments on real-world object classification and scene registration.
- MaskLRF performs well in scenarios where a small number of labeled 3D point sets are available for finetuning, as shown in the experiment on few-shot classification.
- The 3D shape features learned by MaskLRF are useful not only for object-level analysis (i.e., shape classification), but also for point-level dense prediction tasks such as part segmentation and scene registration.
- MaskLRF can learn robust latent features even if there are domain gaps (i.e., synthetic/realistic gap and orientational gap) between training and evaluation data, as shown in the experiment on domain adaptation.

B. FUTURE WORK

This paper proposes the MaskLRF algorithm as the first attempt of the RI MPM framework. However, there is much room for further exploration within the RI MPM framework. Possible future directions include, for example,

- **Using better rotation invariance acquisition methods.** MaskLRF uses the traditional PCA-based LRF to normalize the orientation of local regions. However, the PCA-based LRF is sensitive to noisy 3D points. Therefore, the current MaskLRF may not fulfil its potential in analyzing real-world 3D point sets. To obtain rotation invariance in a more robust way, the use of learning-based LRF (e.g., [43], [47]) or feature extraction DNNs having rotation equivariance (e.g., [38], [39]) should be considered.
- **Pretraining with large-scale and realistic datasets.** The current MaskLRF uses nearly 50,000 synthetic 3D point set data for pretraining. Although its effectiveness was confirmed in the experiments, pretraining with a larger number of data samples may lead to better latent shape features. In addition, pretraining on realistic (not synthetic) 3D point set data is expected to gain robustness against 3D shapes having noisy 3D points, missing parts, and non-uniform point density.
- **Evaluation using more diverse downstream tasks.** The tasks of 3D point set analysis are not limited to classification, part segmentation and scene registration dealt with in this paper. We would like to verify the practicality of the proposed algorithm by evaluating it on additional downstream tasks such as object detection, scene segmentation and shape reconstruction.

REFERENCES

[1] Aoran Xiao, Jiaxing Huang, Dayan Guan, Xiaoqin Zhang, Shijian Lu, Ling Shao, Unsupervised Point Cloud Representation Learning with Deep Neural Networks: A Survey, *IEEE TPAMI*, 2023.

[2] Ben Fei, Weidong Yang, Liwen Liu, Tianyue Luo, Rui Zhang, Yixuan Li, Ying He, Self-supervised Learning for Pre-Training 3D Point Clouds: A Survey, *arXiv preprint*, arXiv:2305.04691, 2023.

[3] Jacob Devlin, Ming-Wei Chang, Kenton Lee, Kristina Toutanova, BERT: Pre-training of Deep Bidirectional Transformers for Language Understanding, *Proc. NAACL 2019*, pp. 4171–4186, 2019.

[4] Kaiming He, Xinlei Chen, Saining Xie, Yanghao Li, Piotr Dollár, Ross Girshick, Masked Autoencoders Are Scalable Vision Learners, *Proc. CVPR 2022*, pp. 16000–16009, 2022.

[5] Zhenda Xie, Zheng Zhang, Yue Cao, Yutong Lin, Jianmin Bao, Zhuliang Yao, Qi Dai, Han Hu, SimMIM: A Simple Framework for Masked Image Modeling, *Proc. CVPR 2022*, pp. 9653–9663, 2022.

[6] Xumin Yu, Lulu Tang, Yongming Rao, Tiejun Huang, Jie Zhou, Jiwen Lu, Point-BERT: Pre-Training 3D Point Cloud Transformers With Masked Point Modeling, *Proc. CVPR 2022*, pp. 19313–19322, 2022.

[7] Haotian Liu, Mu Cai, Yong Jae Lee, Masked Discrimination for Self-supervised Learning on Point Clouds, *Proc. ECCV 2022*, pp. 657–675, 2022.

[8] Yatian Pang, Wenxiao Wang, Francis E.H. Tay, Wei Liu, Yonghong Tian, Li Yuan, Masked Autoencoders for Point Cloud Self-supervised Learning, *Proc. ECCV 2022*, pp. 604–621, 2022.

[9] Renrui Zhang, Ziyu Guo, Rongyao Fang, Bin Zhao, Dong Wang, Yu Qiao, Hongsheng Li, Peng Gao, Point-M2AE: Multi-scale Masked Autoencoders for Hierarchical Point Cloud Pre-training, *Proc. NeurIPS 36*, pp. 27061–27074, 2022.

[10] Yabin Zhang, Jiehong Lin, Chenhang He, Yongwei Chen, Kui Jia, Lei Zhang, Masked Surfel Prediction for Self-Supervised Point Cloud Learning, *arXiv preprint*, arXiv:2207.03111, 2022.

[11] Guangyan Chen, Meiling Wang, Yi Yang, Kai Yu, Li Yuan, Yufeng Yue, PointGPT: Auto-regressively Generative Pre-training from Point Clouds, *Proc. NeurIPS 2023*, 2023.

[12] Ashish Vaswani, Noam Shazeer, Niki Parmar, Jakob Uszkoreit, Llion Jones, Aidan N. Gomez, Lukasz Kaiser, Illia Polosukhin, Attention Is All You Need, *Proc. NeurIPS 30*, pp. 5998–6008, 2017.

[13] Yiyong Sun, Mongi A. Abidi, Surface matching by 3D point's fingerprint, *Proc. ICCV 2001*, pp. 263–269, 2001.

[14] Xiaoyu Tian, Haoxi Ran, Yue Wang, Hang Zhao, GeoMAE: Masked Geometric Target Prediction for Self-Supervised Point Cloud Pre-Training, *Proc. CVPR 2023*, pp. 13570–13580, 2023.

[15] Chen Min, Xinli Xu, Dawei Zhao, Liang Xiao, Yiming Nie, Bin Dai, Occupancy-MAE: Self-supervised Pre-training Large-scale LiDAR Point Clouds with Masked Occupancy Autoencoders, *arXiv preprint*, arXiv:2206.09900, 2022.

[16] Saining Xie, Jiatao Gu, Demi Guo, Charles R. Qi, Leonidas Guibas, Or Litany, PointContrast: Unsupervised Pre-training for 3D Point Cloud Understanding, *Proc. ECCV 2020*, pp. 574–591, 2020.

[17] Zaiwei Zhang, Rohit Girdhar, Armand Joulin, Ishan Misra, Self-Supervised Pretraining of 3D Features on any Point-Cloud, *Proc. ICCV 2021*, pp. 10232–10243, 2021.

[18] Yongming Rao, Benlin Liu, Yi Wei, Jiwen Lu, Cho-Jui Hsieh, Jie Zhou, RandomRooms: Unsupervised Pre-training from Synthetic Shapes and Randomized Layouts for 3D Object Detection, *Proc. ICCV 2021*, pp. 3283–3292, 2021.

[19] Fuchen Long, Ting Yao, Zhaofan Qiu, Lusong Li, Tao Mei, PointClustering: Unsupervised Point Cloud Pre-Training Using Transformation Invariance in Clustering, *Proc. CVPR 2023*, pp. 21824–21834, 2023.

[20] Siming Yan, Yuqi Yang, Yuxiao Guo, Hao Pan, Peng-shuai Wang, Xin Tong, Yang Liu, Qixing Huang, 3D Feature Prediction for Masked-AutoEncoder-Based Point Cloud Pretraining, *arXiv preprint*, arXiv:2304.06911, 2023.

[21] Hanchen Wang, Qi Liu, Xiangyu Yue, Joan Lasenby, Matt J. Kusner, Unsupervised Point Cloud Pre-training via Occlusion Completion, *Proc. ICCV 2021*, pp.9762–9772, 2021.

[22] Zhizhong Han, Xiyang Wang, Yu-Shen Liu, Matthias Zwicker, Multi-Angle Point Cloud-VAE: Unsupervised Feature Learning for 3D Point Clouds from Multiple Angles by Joint Self-Reconstruction and Half-to-Half Prediction, *Proc. ICCV 2019*, pp. 10442–10451, 2019.

[23] Charles R. Qi, Li Yi, Hao Su, Leonidas J. Guibas, PointNet++: deep hierarchical feature learning on point sets in a metric space, *Proc. NeurIPS 31*, pp. 5105–5114, 2017.

[24] Charles R. Qi, Hao Su, Kaichun Mo, Leonidas J. Guibas, PointNet: Deep Learning on Point Sets for 3D Classification and Segmentation, *Proc. CVPR 2017*, pp. 652–660, 2017.

[25] Renrui Zhang, Ziyu Guo, Wei Zhang, Kunchang Li, Xupeng Miao, Bin Cui, Yu Qiao, Peng Gao, Hongsheng Li, PointCLIP: Point Cloud Understanding by CLIP, *Proc. CVPR 2022*, pp. 8552–8562, 2022.

[26] Rui Huang, Xuran Pan, Henry Zheng, Haojun Jiang, Zhifeng Xie, Shiji Song, Gao Huang, Joint Representation Learning for Text and 3D Point Cloud, *arXiv preprint*, arXiv:2301.07584, 2023.

[27] Mohamed Afham, Isuru Dissanayake, Dinithi Dissanayake, Amaya Dharmasiri, Kanchana Thilakarathna, Ranga Rodrigo, CrossPoint: Self-Supervised Cross-Modal Contrastive Learning for 3D Point Cloud Understanding, *Proc. CVPR 2022*, pp. 9892–9902, 2022.

[28] Renrui Zhang, Liuhui Wang, Yu Qiao, Peng Gao, Hongsheng Li, Learning 3D Representations from 2D Pre-trained Models via Image-to-Point Masked Autoencoders, *Proc. CVPR 2023*, pp. 21769–21780, 2023.

[29] Zhimin Chen, Longlong Jing, Yingwei Li, Bing Li, Bridging the Domain Gap: Self-Supervised 3D Scene Understanding with Foundation Models, *Proc. NeurIPS 2023*, 2023.

[30] Alec Radford, Jong Wook Kim, Chris Hallacy, Aditya Ramesh, Gabriel Goh, Sandhini Agarwal, Girish Sastry, Amanda Askell, Pamela Mishkin, Jack Clark, Gretchen Krueger, Ilya Sutskever, Learning Transferable Visual Models From Natural Language Supervision, *Proc. ICML 2021*, pp. 8748–8763, 2021.

[31] Chao Chen, Guanbin Li, Ruijia Xu, Tianshui Chen, Meng Wang, Liang Lin, ClusterNet: Deep Hierarchical Cluster Network With Rigorously Rotation-Invariant Representation for Point Cloud Analysis, *Proc. CVPR 2019*, pp. 4989–4997, 2019.

[32] Zhiyuan Zhang, Binh-Son Hua, David W. Rosen, Sai-Kit Yeung, Rotation Invariant Convolutions for 3D Point Clouds Deep Learning, *Proc. 3DV 2019*, pp. 204–213, 2019.

[33] Xiao Sun, Zhouhui Lian, Jianguo Xiao, SRINet: Learning Strictly Rotation-Invariant Representations for Point Cloud Classification and Segmentation, *Proc. MM 2019*, pp. 980–988, 2019.

[34] Xianzhi Li, Ruihui Li, Guangyong Chen, Chi-Wing Fu, Daniel Cohen-Or, Pheng-Ann Heng, A Rotation-Invariant Framework for Deep Point Cloud Analysis, *TVCG*, Vol. 28, No. 12, pp. 4503–4514, 2022.

[35] Ronghan Chen, Yang Cong, The Devil is in the Pose: Ambiguity-free 3D Rotation-invariant Learning via Pose-aware Convolution, *Proc. CVPR 2022*, pp. 7462–7471, 2022.

[36] Zhiyuan Zhang, Binh-Son Hua, Sai-Kit Yeung, RIConv++: Effective Rotation Invariant Convolutions for 3D Point Clouds Deep Learning, *IJCV*, vol. 130, pp. 1228–1243, 2022.

[37] Chen Zhao, Jiaqi Yang, Xin Xiong, Angfan Zhu, Zhiguo Cao, Xin Li, Rotation Invariant Point Cloud Analysis: Where Local Geometry Meets Global Topology, *Pattern Recognition*, vol. 127, 108626, 2022.

[38] Wen Shen, Binbin Zhang, Shikun Huang, Zhihua Wei, Quanshi Zhang, 3D-Rotation-Equivariant Quaternion Neural Networks, *Proc. ECCV 2020*, pp. 531–547, 2020.

[39] Congyue Deng, Or Litany, Yueqi Duan, Adrien Poulenard, Andrea Tagliasacchi, Leonidas Guibas, Vector Neurons: A General Framework for SO(3)-Equivariant Networks, *Proc. ICCV 2021*, pp. 12180–12189, 2021.

[40] Takahiko Furuya and Ryutarou Ohbuchi, Deep Aggregation of Local 3D Geometric Features for 3D Model Retrieval, *Proc. BMVC 2016*, Vol. 7, p. 8, 2016.

[41] Zelin Xiao, Hongxin Lin, Renjie Li, Hongyang Chao, Shengyong Ding, Endowing Deep 3d Models With Rotation Invariance Based On Principal Component Analysis, *Proc. ICME 2020*, pp. 1–6, 2020.

[42] Feiran Li, Kent Fujiwara, Fumio Okura, Yasuyuki Matsushita, A Closer Look at Rotation-Invariant Deep Point Cloud Analysis, *Proc. ICCV 2021*, pp. 16218–16227, 2021.

[43] Shitong Luo, Jiahan Li, Jiaqi Guan, Yufeng Su, Chaoran Cheng, Jian Peng, Jianzhu Ma, Equivariant Point Cloud Analysis via Learning Orientations for Message Passing, *Proc. CVPR 2022*, pp. 18910–18919, 2022.

[44] Seohyun Kim, JaeYoo Park, Bohyung Han, Rotation-Invariant Local-to-Global Representation Learning for 3D Point Cloud, *Proc. NeurIPS 33*, pp. 8174–8185, 2020.
[45] Junming Zhang, Ming-Yuan Yu, Ram Vasudevan, Matthew Johnson-Roberson, Learning Rotation-Invariant Representations of Point Clouds Using Aligned Edge Convolutional Neural Networks, *Proc. 3DV 2020*, pp. 200-209, 2020.
[46] Jianhui Yu, Chaoyi Zhang, Weidong Cai, Rethinking Rotation Invariance with Point Cloud Registration, *Proc. AAAI 2023*, Vol. 37, No. 3, pp. 3313–3321, 2023.
[47] Dingxin Zhang, Jianhui Yu, Chaoyi Zhang, Weidong Cai, PaRot: Patch-Wise Rotation-Invariant Network via Feature Disentanglement and Pose Restoration, *Proc. AAAI 2023*, pp. 3418–3426, 2023.
[48] Riccardo Spezialetti, Federico Stella, Marlon Marcon, Luciano Silva, Samuele Salti, Luigi Di Stefano, Learning to Orient Surfaces by Self-supervised Spherical CNNs, *Proc. NeurIPS 33*, pp. 5381–5392, 2020.
[49] Seungwook Kim, Yoonwoo Jeong, Chunghyun Park, Jaesik Park, Minsu Cho, SeLCA: Self-Supervised Learning of Canonical Axis, *Proc. NeurIPS 2022 Workshop on Symmetry and Geometry in Neural Representations*, 2022.
[50] Riccardo Spezialetti, Samuele Salti, Luigi Di Stefano, Learning an Effective Equivariant 3D Descriptor Without Supervision, *Proc. ICCV 2019*, pp. 6401–6410, 2019.
[51] Takahiko Furuya, Zhoujie Chen, Ryutarou Ohbuchi, Zhenzhong Kuang, Self-supervised Learning of Rotation-invariant 3D Point Set Features using Transformer and its Self-distillation, *arXiv preprint*, arXiv:2308.04725, 2023.
[52] Alioscia Petrelli, Luigi Di Stefano, On the repeatability of the local reference frame for partial shape matching, *Proc. ICCV 2011*, pp. 2244–2251, 2011.
[53] Jiaqi Yang, Yang Xiao, Zhiguo Cao, Toward the Repeatability and Robustness of the Local Reference Frame for 3D Shape Matching: An Evaluation, *Transactions on Image Processing*, vol. 27, no. 8, pp. 3766–3781, 2018.
[54] Bao Zhao, Xianyong Fang, Jiahui Yue, Xiaobo Chen, Xinyi Le, Chanjuan Zhao, The Z-axis, X-axis, Weight and Disambiguation Methods for Constructing Local Reference Frame in 3D Registration: An Evaluation, *arXiv preprint*, arXiv:2204.08024, 2022.
[55] Jiaqi Yang, Qian Zhang, Yang Xiao, Zhiguo Cao, TOLDI: An effective and robust approach for 3D local shape description, *Pattern Recognition*, Vol. 65, pp. 175–187, 2017.
[56] Du Q. Huynh, Metrics for 3D Rotations: Comparison and Analysis, *Journal of Mathematical Imaging and Vision*, Vol. 35, pp. 155–164, 2009.
[57] Ali Hassani, Humphrey Shi, Dilated Neighborhood Attention Transformer, *arXiv preprint*, arXiv:2209.15001, 2022.
[58] Takahiko Furuya and Ryutarou Ohbuchi, Diffusion-on-Manifold Aggregation of Local Features for Shape-based 3D Model Retrieval, *Proc. ICMR 2015*, pp. 171–178, 2015.
[59] Ilya Loshchilov, Frank Hutter, Decoupled Weight Decay Regularization, *Proc. ICLR 2019*, 2019.
[60] Takahiko Furuya, Xu Hang, Ryutarou Ohbuchi, Jinliang Yao, Convolution on Rotation-Invariant and Multi-Scale Feature Graph for 3D Point Set Segmentation, IEEE Access, vol. 8, pp. 140250-140260, 2020.
[61] Mathilde Caron, Hugo Touvron, Ishan Misra, Hervé Jégou, Julien Mairal, Piotr Bojanowski, Armand Joulin, Emerging Properties in Self-Supervised Vision Transformers, *Proc. ICCV 2021*, pp. 9650–9660, 2021.
[62] Angel X. Chang, Thomas Funkhouser, Leonidas Guibas, Pat Hanrahan, Qixing Huang, Zimo Li, Silvio Savarese, Manolis Savva, Shuran Song, Hao Su, Jianxiong Xiao, Li Yi, Fisher Yu, ShapeNet: An Information-Rich 3D Model Repository, *arXiv preprint*, arXiv:1512.03012, 2015.
[63] Mikaela Angelina Uy, Quang-Hieu Pham, Binh-Son Hua, Duc Thanh Nguyen, Sai-Kit Yeung, Revisiting Point Cloud Classification: A New Benchmark Dataset and Classification Model on Real-World Data, *Proc. ICCV 2019*, pp. 1588–1597, 2019.
[64] Tong Wu, Jiarui Zhang, Xiao Fu, Yuxin Wang, Jiawei Ren, Liang Pan, Wayne Wu, Lei Yang, Jiaqi Wang, Chen Qian, Dahua Lin, Ziwei Liu, OmniObject3D: Large-Vocabulary 3D Object Dataset for Realistic Perception, Reconstruction and Generation, *Proc. CVPR 2023*, pp. 803–814, 2023.
[65] Charu Sharma, Manohar Kaul, Self-Supervised Few-Shot Learning on Point Clouds, *Proc. NeurIPS 34*, pp. 7212–7221, 2020.
[66] Zhirong Wu, Shuran Song, Aditya Khosla, Fisher Yu, Linguang Zhang, Xiaoou Tang, Jianxiong Xiao, 3D ShapeNets: A Deep Representation for Volumetric Shapes, *Proc. CVPR 2015*, pp. 1912–1920, 2015.
[67] Li Yi, Vladimir G. Kim, Duygu Ceylan, I-Chao Shen, Mengyan Yan, Hao Su, Cewu Lu, Qixing Huang, Alla Sheffer, Leonidas Guibas, A Scalable Active Framework for Region Annotation in 3D Shape Collections, *ACM ToG*, Vol. 35, Issue 6, Article No. 210, pp 1–12, 2016.
[68] Hao Yu, Ji Hou, Zheng Qin, Mahdi Saleh, Ivan Shugurov, Kai Wang, Benjamin Busam, Slobodan Ilic, RIGA: Rotation-Invariant and Globally-Aware Descriptors for Point Cloud Registration, *arXiv preprint* arXiv:2209.13252, 2022.
[69] Hao Yu, Zheng Qin, Ji Hou, Mahdi Saleh, Dongsheng Li, Benjamin Busam, Slobodan Ilic, Rotation-Invariant Transformer for Point Cloud Matching, *Proc. CVPR 2023*, pp. 5384–5393, 2023.
[70] Andy Zeng, Shuran Song, Matthias Nießner, Matthew, Fisher, Jianxiong Xiao, and Thomas Funkhouser. 3DMatch: Learning Local Geometric Descriptors from RGB-D Reconstructions. *Proc. CVPR 2017*, pp. 1802–1811, 2017.
[71] Shengyu Huang, Zan Gojcic, Mikhail Usvyatsov, Andreas Wieser, Konrad Schindler, Predator: Registration of 3D Point Clouds With Low Overlap, *Proc. CVPR 2021*, pp. 4267–4276, 2021.
[72] Haowen Deng, Tolga Birdal & Slobodan Ilic, PPF-FoldNet: Unsupervised Learning of Rotation Invariant 3D Local Descriptors, *Proc. ECCV 2018*, pp. 620–638, 2018.
[73] Haiping Wang, Yuan Liu, Zhen Dong, and Wenping Wang, You Only Hypothesize Once: Point Cloud Registration with Rotation-equivariant Descriptors, *Proc. ACM MM 2022*, pp. 1630–1641, 2022.
[74] Zheng Qin, Hao Yu, Changjian Wang, Yulan Guo, Yuxing, Peng, and Kai Xu, Geometric Transformer for Fast and Robust Point Cloud Registration, *Proc. CVPR 2022*, pp. 11143–11152, 2022.
[75] Can Qin, Haoxuan You, Lichen Wang, C.-C. Jay Kuo, Yun Fu, PointDAN: A Multi-Scale 3D Domain Adaption Network for Point Cloud Representation, *Proc. NeurIPS 33*, pp. 7192–7203, 2019.
[76] Idan Achituve, Haggai Maron, Gal Chechik, Self-Supervised Learning for Domain Adaptation on Point Clouds, *Proc. WACV 2021*, pp. 123–133, 2021.
[77] Longkun Zou, Hui Tang, Ke Chen, Kui Jia, Geometry-Aware Self-Training for Unsupervised Domain Adaptation on Object Point Clouds, *Proc. ICCV 2021*, pp. 6403–6412, 2021.
[78] Hanxue Liang, Hehe Fan, Zhiwen Fan, Yi Wang, Tianlong Chen, Yu Cheng, Zhangyang Wang, Point Cloud Domain Adaptation via Masked Local 3D Structure Prediction, *Proc. ECCV 2022*, pp. 156–172, 2022.
[79] Yuefan Shen, Yanchao Yang, Mi Yan, He Wang, Youyi Zheng, Leonidas J. Guibas, Domain Adaptation on Point Clouds via Geometry-Aware Implicits, *Proc. CVPR 2022*, pp. 7223–7232, 2022.
[80] Hehe Fan, Xiaojun Chang, Wanyue Zhang, Yi Cheng, Ying Sun, Mohan Kankanhalli, Self-Supervised Global-Local Structure Modeling for Point Cloud Domain Adaptation with Reliable Voted Pseudo Labels, *Proc. CVPR 2022*, pp. 6377–6386, 2022.
[81] Joonhyung Park, Hyunjin Seo, Eunho Yang, PC-Adapter: Topology-Aware Adapter for Efficient Domain Adaption on Point Clouds with Rectified Pseudo-label, *Proc. ICCV 2023*, pp. 11530–11540, 2023.

TAKAHIKO FURUYA received his Ph.D. degree in information and systems engineering from University of Yamanashi, Japan, in 2015. Currently, he is an associate professor at Integrated Graduate School of Medicine, Engineering, and Agricultural Sciences, University of Yamanashi. His research interest includes multimedia information retrieval, 3D shape analysis, computer vision, and machine learning.